Introducing a Cellular Automaton as an Empirical Model to Study Static and Dynamic Properties of Molecules Adsorbed in Zeolites

Pierfranco Demontis,* Federico G. Pazzona, and Giuseppe B. Suffritti

Dipartimento di Chimica, Università degli Studi di Sassari and Consorzio Interuniversitario Nazionale per la Scienza e Tecnologia dei Materiali (INSTM), Unità di Ricerca di Sassari, via Vienna, 2, I-07100 Sassari, Italy

Received: June 16, 2008; Revised Manuscript Received: August 5, 2008

A new lattice gas cellular automaton (LGCA) simulation approach to study static and dynamic properties of molecules adsorbed in zeolites is proposed. The motivation for the present work arises from the ongoing effort to develop efficient numerical tools where conventional approaches like molecular dynamics and Monte Carlo have been revealed as inefficient for a real extension of length and time scales in such inhomogeneous systems. Our LGCA is constituted by a constant number of interacting identical particles, distributed among a fixed number of identical cells arranged in a three-dimensional cubic network and performing a synchronous random walk at constant temperature. The main input for our model comes from data such as (i) local density dependent mean-field potentials and transition probabilities obtained from atomistic simulations that will be used as the starting point to derive adsorption and diffusion properties and (ii) thermodynamic and kinetic data obtained from experiments and/or other simulation methods. Our numerically less demanding LGCA has been tested over three different systems. The obtained results are in excellent agreement with the experimental and theoretical reported data.

1. Introduction

In industrial processes, zeolites and related silicate molecular sieves have found wide application as catalysts, sorbents, and ion-exchangers.[1] The commercial interest for this kind of materials is constantly increasing, and new fields of utilization have been predicted in the near future.[2] Application of fundamental scientific principles to the key technological issues involved has been difficult, however, and much more progress has been attained through exploitation of empirical processing parameters than through a deep understanding of the chemical and physical mechanisms that control catalytic activity, sorption, and diffusion.[1]

Advanced experimental research in this field is often very expensive and time-consuming; moreover the interpretation of the results is not always unambiguous. This gives rise to the quest for the development of reliable theoretical and computational methods to significantly contribute to the microscopic understanding of phenomena in a microporous environment. The starting point for any model at molecular level is a proper description of the microstructure of the zeolite that is generally provided by experimental crystal structure determination.[3,4] Then this collection of atoms and ions (fixed in space or moving according to a suitable interaction potential) is linked to a description of the intermolecular forces through which adsorbed molecules interact with the inner surface and with each other. This is the conventional approach based on empirical potentials. Recent developments in algorithms combined with the use of increasingly faster computers are extending the realm of applicability of first principles atomistic calculations for predicting performance and properties of microporous materials.[5] So far Monte Carlo (MC)[6] and molecular dynamics (MD)[7] techniques are the most widely used tools in the molecular modeling of adsorption and diffusion in zeolites. MC simulations are used mainly to study the thermodynamics of molecules adsorbed in zeolites. Predictions of adsorption isotherms and heats of adsorption are generally in good agreement with experimental results. The simulations also provide interesting details about the molecular-level arrangement of the molecules within the zeolite pores. This information has proven very useful in explaining the complex behavior of molecules in tight confinement.[8] In addition to thermodynamics the details of the molecular motion are promptly available from MD simulations so that the mechanism of diffusion can be studied.[9,10] In principle, MD simulations could investigate any classical problem at a molecular level, but the wide range of diffusional time scales encountered by molecules in zeolites limits the applicability of MD to processes that occur on the order of femto- to nanoseconds.[11] When in the zeolite the sorption sites are separated by large free energy barriers compared to thermal energies a slowdown of molecular motion is observed. In this regime the intrinsic time-scales of the dynamic events are not amenable to direct MD simulation using present computer technology and transition state theory (TST) and related methods must be used to simulate the temperature dependence of site-to-site jump rate constants. Under these conditions other methods become more suitable by replacing the crystal lattice with a three-dimensional lattice of binding sites, and kinetic Monte Carlo (KMC) and mean field theory can be employed to model the loading dependence of activated diffusion in zeolites.[12,13]

By applying these methods the main question becomes: can a simple, space-time discrete model properly describe at the macroscopic scale the features of diffusion in microporous materials such as zeolites? The answer should be yes if the parameters governing the thermodynamic and kinetic behaviors are properly set. This is because a lattice model works with a drastically reduced number of degrees of freedom, in order to cover large scales on space and time. The main task is then to find how to transfer the essential physical features of molecules adsorbed inside micropores (as they are obtained from atomistic

* Corresponding author. Phone: +39 079 229 551. Fax: +39 079 229 559. E-mail: demontis@uniss.it.

10.1021/jp805300z CCC: $40.75
Published on Web 09/06/2008

simulations or from experiments) to the parameters defining the local properties of each cage or channel and to use such a coarse-grained description as a tool to perform large-scale simulations of the zeolitic material of interest.

In the literature, there are several thermodynamic lattice models attempting to describe the equilibrium properties of a fluid adsorbed inside of a zeolite or, more generally, inside of a discretized framework such as an arbitrary microporous material or a solid surface. In some models, the thermodynamics of a lattice is represented through the properties of a single, open cell treated as a small grand-canonical system and able to host a limited number of particles. The approaches to obtain the cellular statistical properties range from the development of a grand-canonical partition function formalism[14−16] to the formulation of conditional probability distribution functions of hard spheres.[17,18] In both cases, interactions between the adsorbed particles are represented by a mean field potential, which can be a fixed mean interaction,[17,18] or a function of the occupancy of the single cell[14,15] (the number of particles adsorbed which is a discrete, local observable) or a function of the loading[16] (average occupancy, a continuous global observable). The strength of such models stands in their very simple way to take account of molecular interactions by introducing local potentials in a simple parametric form. Some models can be used to fit adsorption isotherms[15,16] and some others to fit occupancy distribution functions.[14,17,18] The main drawback is that they contain no kinetic information.

On the contrary, KMC models are focused on the migration rates from site to site in a lattice, in order to reproduce diffusion properties of molecular species.[19−23] When improved with the introduction of the correct jump rates and transmission factors obtained from MD simulations, such models can be coupled with TST and then become quantitatively able to reproduce the self-diffusivity profiles of adsorbed species in zeolites.[24,25] However, KMC models are not aimed at the accurate reproduction of equilibrium properties.

Cellular automata (CAs)[26−28] are discrete dynamical systems where space is represented by a uniform grid with each cell containing a few bits of data, and local and homogeneous laws allow the system to evolve in discrete time steps of fixed duration. Due to their discreteness and the absence of truncations or approximations in their dynamics, CAs evolve without being affected by numerical instabilities. Moreover, on the analogy of MD, a cellular automaton (CA) model is an implementation of a *N*-body system where all correlations are taken into account, fluctuations arise spontaneously, and due to time homogeneity CA observables can be monitored in the same way as in MD simulations. However it is important to note that a proper care of correlations must be taken into account because in discrete models they may be stronger than in the continuous counterpart.[29] CAs are widely used as a modeling tool in natural science, combinatorial mathematics, and computer science. With their simple structure, they represent a natural way of studying the evolution of large physical systems under both equilibrium and nonequilibrium conditions.[30,31]

The goal of the present work has been to develop a possible framework for such a coarse-grained approach to molecular adsorption and diffusion in microporous environments. We built a lattice-gas cellular automaton (LGCA) model[26,32−34] for the description of such processes in the framework of an equilibrium block cellular automaton (BCA)[27,35] which incorporates both the easy-to-tune cellular statistics as made available by thermodynamic lattice models, and the correct long-time kinetic behavior obtainable by MD and KMC. The simple and flexible parametric structure of our BCA makes it exploitable in the wide range of problems connected to molecular adsorption, diffusion and related processes in microporous materials.

In our method a grid of connected cells replaces the underlying crystalline regular structure and the molecules are described as point particles that move on this grid.

The main input for our model comes from data like (i) local density dependent mean-field potentials and transition probabilities obtained from atomistic simulations that will be used as the starting point to derive adsorption and diffusion properties and (ii) thermodynamic and kinetic data obtained from experiments and/or other simulation methods, used as the starting point of a fit procedure aimed to trace which local behaviors cause the system to produce them, or aimed to further enlarge the scales. In what follows we will show how local parameters can be manipulated to make the CA able to fit very well given adsorption and diffusion data. After a brief outline of the basic concepts in section 2, three cases will be considered as illustrative applications of the methodology in section 3. We shall present numerical results for the following systems:

- Xenon atoms in NaA zeolite, where we modeled the interactions in order to fit equilibrium properties avaiable from both experimental measurements and grand-canonical Monte Carlo (GCMC) simulations of Jameson et al.,[36,37] without an explicit modeling of the kinetics.
- Methane in ZK4 zeolite, where we modeled the particle-framework interactions and the kinetics in order to fit MD results relevant to equilibrium properties from Fritzsche et al.[38] and self-diffusivities from Dubbeldam et al.[24] while neglecting the interparticle interactions.
- Ethylene in NaA zeolite, where we modeled both interactions and kinetics to fit adsorption and self-diffusion data from experimental results of Ruthven and Derrah[39] and from a lattice model developed by Gladden et al.[40]

2. The Model

2.1. Structure and Thermodynamics. In this work three different examples of species adsorbed in Linde type A (LTA) zeolites (namely, NaA and ZK4) are illustrated.[3] The LTA framework consists of a cubic array of nearly spherical cavities (α-cages) with an internal radius ρ of about 5.7 Å, each one connected to six neighboring cavities by nearly circular windows of about 4.2 Å in diameter. Such a framework has been modeled as a grid of M cubically arranged cells (each one representative of one α -cage) with homogeneous lattice spacing $\lambda = 2\rho$ and periodic boundary conditions, in which N mutually exclusive particles (Xe atoms and methane or ethane molecules) may diffuse at constant temperature by jumps between neighboring cells. The loading $\bar{n}$ of the system is defined as the average number of particles per cell, that is $\bar{n} = N/M$.

Each cell is made of $K = K_{ex} + K_{in}$ sites, each one able to host one particle, where K_{ex} and K_{in} indicate respectively the number of exit sites (allowing intercell transfers) and inner sites (not allowing such transfers). This fixes at K the maximum occupancy of the cell. Each exit site is associated to the access to one of the six windows connecting the real α-cage to one of its six neighboring cages, so it can be interpreted as a discrete representation of the location inside of the α-cage, close to the window. Since for xenon as well as for methane and ethane a window of a LTA zeolite can be passed by only one particle at a time, we include this constraint on the particle traffic into our model by associating only one exit site to each window (i.e., $K_{ex} = 6$). Inner sites are structureless, for they represent all of the locations of the real α-cage not allowing access to a window.

In the present model, other details about the internal structure of the cell are not defined.

The instantaneous position of each particle in the grid is defined as the coordinates of its current host cell (the analog of the coordinates of the center of the real α-cage), taking account of periodic boundary conditions. The entire system evolves through discrete time steps of duration τ. Once an accurate fit of normalized diffusion properties has been obtained, a precise value of the constant τ may be rendered explicit a posteriori to provide connection between real and simulated time scale. However, since that adds no further information about the model's behavior, we choose to keep τ implicit.

Our model is strictly local at the cellular level; that is, we assume interparticle interactions to be short-ranged so that intercell interactions are negligible. The energetics of each cell is defined in such a way as to allow the local observables n_{ex} (the number of occupied exit sites) and n_{in} (the number of occupied inner sites) to define completely the instantaneous state of the cell, denoted as (n_{ex},n_{in}). Moreover the transfer between two neighboring cells may be affected by a local diffusion barrier which depends on the actual states of the two cells involved in the exchange process.

The model simulates adsorption and diffusion in the canonical ensemble. Indicating with $a = \{a_0, \ldots, a_K\}$ a distribution of occupancies (that is, a_n indicates the number of cells containing n particles) and with $T = (k_B\beta)^{-1}$ the temperature of the system (k_B is the Boltzmann's constant), the canonical partition function of the model reads

$$Q^{sys}(N;\beta) = M! \sum_{a} \prod_{n=0}^{K} \frac{[Q(n;\beta)]^{a_n}}{a_n!} \tag{1}$$

where the sum runs over all possible distributions of occupancies satisfying[41] $\sum_n a_n = M$ and $\sum_n n a_n = N$. In eq 1, a central role is played by the (canonical) local partition function of a n-occupied cell

$$Q(n;\beta) = \sum_{n_{ex}=0}^{K_{ex}} \sum_{n_{in}=0}^{K_{in}} \delta_{kr}(n_{ex}+n_{in},n) \prod_{s=ex,in} \binom{K_s}{n_s} [q_s(n;\beta)]^{n_s} \tag{2}$$

where $\delta_{kr}(n_{ex}+n_{in},n)$ is a Krönecker delta restricting the sum to the values of n_{ex} and n_{in} preserving the cell occupancy n.

The quantity $q_s(n;\beta)$ represents the partition function of a particle in a site[16] of type s (which can be "ex" or "in" whether it is an exit or inner site, respectively) at the given temperature when the cell occupancy is n. With such a definition, it is assumed q_s to contain all of the locally averaged contributions to the particle's free energy in the cell, including those arising from particle-framework and particle−particle interactions, accessible volume and presence of cations as in the case of the NaA zeolite. It is appropriate to remark that inside the real α-cages the dependence of the accessible volume on the local density represents an essential feature of confinement. The associated free energy is (from now on, we will drop the independent variable β for simplicity of notation)

$$f_s(n) = -\beta^{-1} \ln q_s(n) = f_s^o + \varphi_s(n) \tag{3}$$

The parameter f_s^o plays the role of an effective adsorption energy of a particle adsorbed in a site of type s when no other particles are hosted in the cell. The difference $\Delta f(n) = f_{ex}(n) - f_{in}(n)$ determines the accessibility of the exit sites in a n-occupied cell, therefore affecting its thermodynamic tendency to release particles to the neighboring cells. The free energy $\phi_s(n)$ can be thought as an effective interaction energy per particle. If we define the free energy of the configuration (n_{ex},n_{in}) as

$$F(n_{ex},n_{in}) = n_{ex} f_{ex}(n) + n_{in} f_{in}(n) \tag{4}$$

then the productory in eq 2 can be written as

$$\prod_{s=ex,in} \binom{K_s}{n_s} [q_s(n;\beta)]^{n_s} = \binom{K_{ex}}{n_{ex}} \binom{K_{in}}{n_{in}} \exp\{-\beta F(n_{ex},n_{in})\} \tag{5}$$

For the sake of simplicity, in the present work we shall assume $\phi_{ex} = \phi_{in} \equiv \phi$. In this way the accessibility of the exit sites is entirely ruled by the difference $\Delta f^o = f^o_{ex} - f^o_{in}$. The more general case of $\phi_{ex} \neq \phi_{in}$ will be the subject of future investigations.

We remark that, although the global partition function $Q^{sys}(N)$ in eq 1 is a summation of a very large (but, in principle, countable) number of terms, its mathematical structure is simple and its value is completely determined by the local partition functions $Q(n)$. Therefore while the evolution of the entire system is simulated in the canonical ensemble, each single cell inside the system obeys the statistics of the grand-canonical ensemble, i.e. the probability of a cell to have occupancy n satisfies[33,41] $p^{eq}(n) \propto \exp(\beta\mu n)\ Q(n)$. Then the chemical potential at any given loading can be calculated through

$$\exp(-\beta\mu) = \frac{p^{eq}(n)}{p^{eq}(n+1)} \frac{Q(n+1)}{Q(n)} = \frac{p^{eq}(n-1)}{p^{eq}(n)} \frac{Q(n)}{Q(n-1)} \tag{6}$$

valid for $n = 1, \ldots, K-1$ (we note that for the case $n = 0$ only the first equality is defined, whereas for $n = K$ only the second one is). In the equalities (6) the probabilities p^{eq} are obtained from numerical simulations in the long-time limit at a given loading $\bar{n}$, while the local partition functions Q are given by eq 2. Therefore the cellular locality allows to compute both equilibrium and transport properties all at once from simulations in the canonical ensemble, without the need of performing separated grand-canonical simulations to obtain adsorption isotherms.

The local partition function $Q(n)$ is strictly connected to the free energy function $f_s(n)$. Therefore, due to the cellular locality of interactions (see eq 3), $f_s(n)$ controls the thermodynamic properties of the entire system. Such a strict locality is a key feature giving the model a high "tunability" to mimic a wide range of real systems of locally interacting molecules.

2.2. Time Evolution. Here we summarize briefly the evolution rules of the model.

At each time step, two operations are performed on the cells of the system: randomization and propagation. In Figure 1 an example of such operations is reported. During randomization, the input cell state defined by $A = (n_{ex},n_{in})$ may be turned into a new one $B = (m_{ex},m_{in})$ with probability

$$p^{rand}(A \rightarrow B) = \binom{K_{ex}}{m_{ex}} \binom{K_{in}}{m_{in}} \frac{\exp\{-\beta F(m_{ex},m_{in})\}}{Q(n_{ex}+n_{in})} \tag{7}$$

provided that occupancy is preserved, i.e., $m_{ex} + m_{in} = n_{ex} + n_{in}$. Next, m_{ex} and m_{in} particles are randomly placed in the exit and the inner sites respectively. The randomization is synchronously performed on all of the M cells of the system.

In order to illustrate the propagation operation, we consider a pair of adjacent cells, called left cell (**L**) and right cell (**R**), connected via the respective exit sites tagged as l and r. Let **L** be in the state (n_{ex},n_{in}) and **R** be in the state (m_{ex},m_{in}) after randomization. **L** and **R** are connected by two adjacent exit sites:

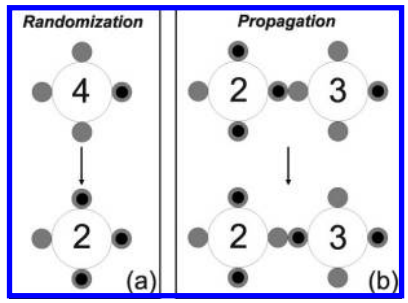

Figure 1. Schematic picture of evolution operations on the system (cross sections). (a) Example of randomization on a single cell. Particles in the exit sites are represented through black dots, while big numbers inside the white circles indicate the number of particles residing in the inner sites. A transition from an input (up) to an output configuration (down) occurs with probability p^{rand} given by eq 7. (b) Propagation on a pair of neighboring cells. A particle jump between two adjacent exit sites is accpeted with probability p^{prop} given by eq 8.

if they are both occupied, the free-energy barrier to intercell migration is infinite[42,43] and no transfer can occur; if only one is occupied, then the barrier is finite and the occupying particle may try to overcome it in order to jump into the adjacent empty site.

In the case of a successful jump, the state of the pair of cells will change.

- Cell **L** transition: $(n_{\text{ex}},n_{\text{in}}) \rightarrow (n_{\text{ex}} - 1,n_{\text{in}})$;
- Cell **R** transition: $(m_{\text{ex}},m_{\text{in}}) \rightarrow (m_{\text{ex}} + 1,m_{\text{in}})$.

Hence the free energy of the particles adsorbed in the sites of **L** and **R** will change from

$$F(C) = F(n_{\text{ex}}, n_{\text{in}}) + F(m_{\text{ex}}, m_{\text{in}})$$

to

$$F(D) = F(n_{\text{ex}} - 1, n_{\text{in}}) + F(m_{\text{ex}} + 1, m_{\text{in}})$$

We use $F(C)$ and $F(D)$ as a starting point to define a propagation probability satisfying detailed balance. Many schemes are possible, giving slightly different kinetic behaviors. Within the present example, the scheme we propose here is the following:

$$p^{\text{prop}}(C \rightarrow D) = \frac{e^{-\beta F(D)} e^{-\beta \epsilon(C,D)}}{e^{-\beta F(C)} + e^{-\beta F(D)}} \tag{8}$$

where $\epsilon(C,D) = \epsilon(D,C) \geq 0$ can be defined as a local kinetic barrier to rescale the transition probability given in eq 8 to provide connection with the real transfer rate[44] (with "local" we mean "dependent on local observables"). The kinetic barrier ϵ adds to the thermodynamic barrier, which is the barrier determined by the detailed balance requirement (eq 8 without the term $e^{-\beta\epsilon(C,D)}$) and its definition depends on the particular case under study: (i) If reference dynamic data are not available, ϵ can be treated as a constant. (ii) In order to gain quantitative agreement with diffusion data, ϵ can be defined through direct coarse-graining of available atomistic data as a function of many local observables related to both cells involved in propagation. (iii) In the absence of detailed information about the real local transfer rates (i.e., this work), the barrier ϵ should be defined in an empirical way.

For this purpose we introduce an occupancy-dependent effective barrier[44] between pre- and postpropagation configurations. To illustrate it, we shall examine the case of a particle jumping from cell **L** to **R**; therefore, let us suppose site l to contain one particle and site r to be empty. To define the configurations we introduce the notation $\{n,j,m\}$. Here, n and m are the occupancies of cells **L** and **R**, respectively, and j is the occupancy of a hypothetical higher free energy transition state where the leaving particle is exactly at the top of the barrier between the cell **L** and the cell **R**. Along with this notation,

- $\{n,0,m\}$ is the prepropagation configuration;
- $\{n - 1,1,m\}$ is the transition state configuration;
- $\{n - 1,0,m + 1\}$ is the postpropagation configuration.

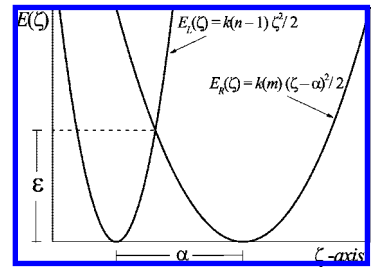

Figure 2. Harmonic model of the kinetic barrier ϵ, defined as the parabola intersection energy.[45,44] In the present example, $k(n - 1) > k(m)$.

In this work, we define the kinetic barrier as a composition of harmonic barriers[45,46] in configuration space as shown in Figure 2. In this space we introduce ζ,α, and the function $k = k(n)$ (with $n = 0, \ldots, K - 1$) respectively as a coordinate (independent variable), a "distance" parameter, and an occupancy-dependent force constant. Then, we define $\epsilon = \epsilon(\{n - 1,1,m\})$ as the intersection point (for $0 < \zeta < \alpha$) between two harmonics $E_{\mathbf{L}}(\zeta)$ and $E_{\mathbf{R}}(\zeta)$ connected to the transition state configuration $\{n - 1,1,m\}$

$$E_{\mathbf{L}}(\zeta) = k(n-1)\zeta^2/2 \tag{9}$$

$$E_{\mathbf{R}}(\zeta) = k(m)(\zeta - \alpha)^2/2 \tag{10}$$

With this formalism, it turns out that the transition state configurations of a jump and of its reverse are equal, i.e., $\epsilon(\{n - 1,1,m\}) = \epsilon(\{m,1,n - 1\})$, and the domain of the function k is relatively small (namely, K points). The usage of more general approaches, such the direct modeling of ϵ as a function of both left and right occupancies n and m, is recommended only to perform a coarse-graining of microscopic data, such as the rate of transfer of a particle between two cages with occupancies n and m.

The BCA approach allows an interacting CA to reach thermodynamic equilibrium. BCAs are also known as "partitioning cellular automata", since they are set up to perform some operations (the propagation in the present case) by making use of a partitioning scheme which subdivides the grid into different partitions of nonoverlapping blocks (here 1 block = 1 pair of adjacent cells). The key idea is that, due to the locality of the evolution laws, all of the blocks belonging to the same partition can undergo the propagation synchronously, and the partitions are switched in a random sequence in order for each cell to communicate with all of its 6 neighbors at each time step, without introducing memory effects. A clear and detailed presentation of this methodology can be found in the works of Toffoli and Margolus.[27,35]

3. Numerical Simulations

All of the numerical simulations in this work have been performed on a lattice of $32 \times 32 \times 32$ cells, for a total observation time of 10^6 time steps after an equilibration time between 10^3 and 2×10^4 time steps, depending on the average intercell transfer rate of particles. All input parameters of the simulations are listed in Table 1.

TABLE 1: All BCA Parameters Used in This Work to Fit Data from Literature[a]

	Xe in NaA	CH_4 in ZK_4	C_2H_4 in NaA	
n	$\phi(n)$	$k(n)$	$\phi(n)$	$k(n)$
0		18		3.5
1	0	18	0	11
2	−0.3309	18	−0.2672	11.5
3	−0.9057	18	−0.5494	9
4	−1.3248	21	−0.7848	1.3
5	−1.5085	21	−0.9763	0.5
6	−1.2631	21	−0.1333	0
7	−0.7891	0	+∞	
8	−0.1603	2	+∞	
9		2.5		
10		12.8		
11		28		
12		30		
13		26		
14		19		

[a] See text for details. Values for the parameter ϕ are expressed in units of kJ mol^{-1}. All reported values of the force constant $k(n)$ refer to $\alpha = 1$.

3.1. Application: Xenon in Zeolite NaA. We modeled our automaton in order to reproduce the adsorption isotherm of xenon in zeolite NaA at 300 K reported by Jameson et al.[36] (experimental and GCMC simulation data). The obtained parameters produced equilibrium probability distributions of occupancies in quantitative agreement with experimental NMR results.[37]

In this application we choose not to treat cations as particles inside the cells; their presence is taken into account in an implicit way by fixing the maximum occupancy at $K = 8$[36,37] (instead of 15 as it would be in a cation-free zeolite like ZK4).[47] According to the cell structure defined in section 2.1, only the topology of the $K_{ex} = 6$ exit sites is defined in an octahedral arrangement as confirmed by measurements of Lim et al.,[48] which justifies the cubic topology of the entire grid of cells. The remaining $K - K_{ex} = 2$ sites are taken as structureless inner sites, referring to locations of a real zeolite cell which are not necessarily close to the center of an α-cage (where no Xe atom was found in any of the measurements of Jameson et al.),[36,37,49,50] but simply they represent locations which do not give access to any of the 6 windows. In order to mimic the effect of window blocking,[51] we assume that all exit sites are available but (i) their accessibility is less than the inner sites (this is achieved by setting $f^o_{in} < f^o_{ex}$) and (ii) they are affected by a mean field diffusion barrier ϵ (see eq 8) that scales by a factor $e^{-\beta\epsilon} = 0.1$ the escape probability of a particle close to a window, therefore inducing a homogeneous slowdown of the diffusion process.[34] Since we are at present interested in obtaining a qualitative diffusivity trend, ϵ is treated as a fixed parameter. An adsorption isotherm is a valuable source of information with regard to the peculiar features of a host−guest system, since it describes quantitatively the amount of gas adsorbed by a porous material at a fixed temperature as a function of pressure (or chemical potential). As in microporous materials where the filling of micropores is ruled by the stronger interactions between the adsorbate molecules and the pore walls, the shape of an isotherm can be exploited to extract information about these forces. Therefore, a strategy to find the best values of f^o_s and ϕ would be to use mean field equations (obtainable following the same route of our previous works[33,34]) to (i) extract the values of f^o_s providing a good fit of the isotherm for low loadings under the approximation of noninteracting LGCA and to (ii) introduce the interaction ϕ as a correction function, in order to mimic repulsive/attractive effects which improve the fit for higher loadings.

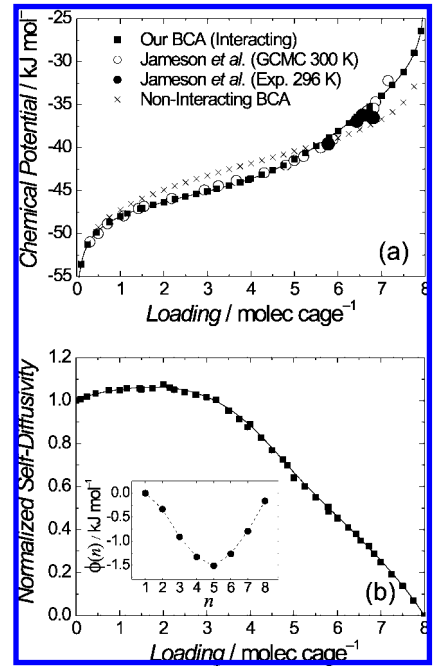

Figure 3. (a) Adsorption isotherm of Xe in NaA zeolite at 300 K obtained by introducing the effective parameters shown in Table 1 into our BCA, in direct comparison with GCMC and experimental results from Jameson et al.,[36] taken as the reference data to fit. The adsorption isotherm of a noninteracting lattice-gas[33] characterized by the same values of K, f^o_{ex}, and f^o_{in} is also shown. In (b) the resulting BCAs diffusivity trend (normalized wrt the diffusivity in the limit of infinite dilution) is shown together with a picture of the trend of the fitting parameter ϕ (inset).

Both the reference isotherm and an excellent fitting curve can be found in Figure 3a. In the same figure we report the adsorption isotherm for a noninteracting lattice gas characterized by the same structure and by the values of the free energy parameters $f^o_{ex} = -41.920$ kJ mol^{-1} and $f^o_{in} = -44.920$ kJ mol^{-1} providing the best fit to the reference data. In Figure 3b we reported the obtained trend of self-diffusivity vs loading and of the interaction function ϕ vs occupancy n (inset). All of the obtained values of parameters are listed in Table 1.

We note (inset of Figure 3b) that ϕ reaches a minimum at intermediate values of n and then increases again due to repulsion. This finding is in qualitative agreement with (i) the trend of the average energy of clusters of n Xe atoms inside NaA zeolite cavities as obtained by Li and Berry[52] through atomistic simulations and (ii) the interaction potentials of previous thermodynamic models by Ayappa[16] and Cheung.[14]

As can be seen in Figure 3b, the obtained self-diffusivity profile exhibits small variations up to loading $\bar{n} = 3$, and then decreases until it goes to zero at the saturation limit $\bar{n} = 8$. Such a trend corresponds to the type-II of the profiles observed by Kärger and Ruthven in the pulsed field gradient-NMR (PFG-NMR) measurements of intracrystalline self-diffusion coefficient depending on sorbate concentration.[53] Therefore, although our model is simple in its structure and in this application the kinetic parameter ϵ is homogeneous, the (qualitative) diffusive behavior it produces is meaningful. This represents an improvement over the lattice model of Jameson et al.[37] (where the trend is monotonically increasing near saturation, which is unphysical for the problem of diffusion in zeolites), and over the models of Ayappa[16] and Cheung[14] which provide no diffusivity trend.

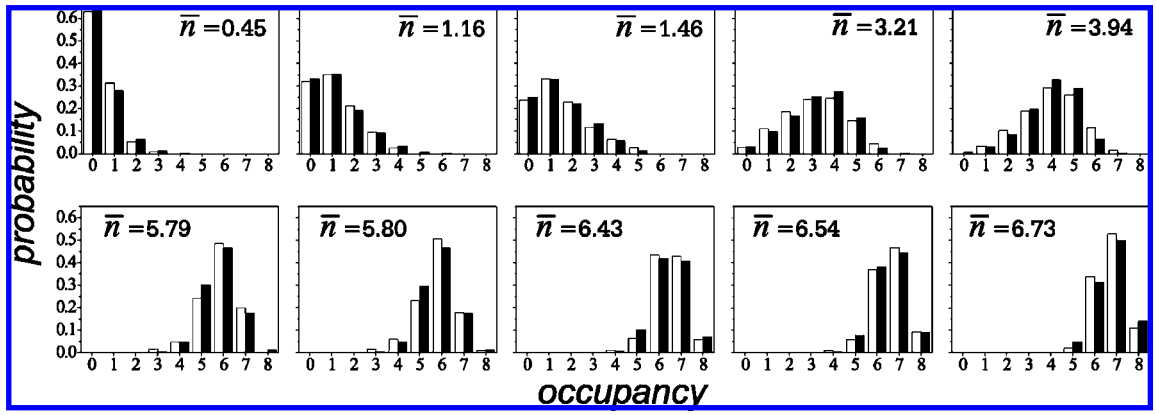

Figure 4. Occupancy probability distributions of particles in the cells from numerical simulations of our BCA (black bars) for Xe in NaA zeolite are shown for various loadings in direct comparison with experimental results of Jameson et al.[37] (white bars).

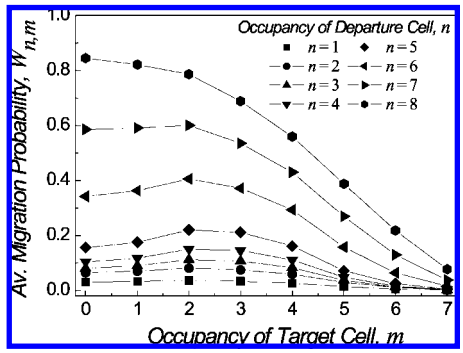

Figure 5. Average probability of a *n*-occupied cell to release a particle to a neighboring *m*-occupied cell. The line serves only as a guide for the eye. Each curve corresponds to a particular value of the occupancy of the departure cell.

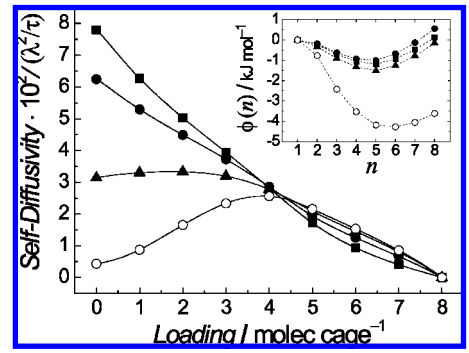

Figure 6. BCAs diffusivity trends connected with the same set of partition functions fitting the isotherm of Xe in NaA, but arising from different values of Δf^o, i.e., changing the relative accessibility of inner and exit sites: (○) $\Delta f^o = 10$, (▲) $\Delta f^o = 4$, (●) $\Delta f^o = 0$, (■) $\Delta f^o = -4$. (All values are in units of kJ mol^{-1}.) In the inset the trends of ϕ preserving the partition function $Q(n)$ are shown.

In Figure 4 it is shown that the obtained free energy parameters give the same probability distributions of particles in the α -cages at different loadings as obtained experimentally.[49] This is a remarkable result. Our BCA after a proper setting of its internal parameters is able to describe the nature of the equilibrium distributions of xenon atoms trapped inside the α-cages. Therefore, it represents an alternative to lattice MC calculations[37] to get a quantitative explanation of ^{129}Xe chemical shifts obtained by NMR measurements.[49] Consequently, we have the reasonable expectation that the very good agreement obtained in the description of the spatial distribution could be extended to the cage-to-cage migration process of the adsorbed fluid in the zeolite by using the same parameters.

In order to confirm such expectations, we computed the average migration probability, $W_{n,m}$, of a particle to migrate from an *n*- to an *m*-occupied neighboring cell during propagation. In our model such a quantity is independent of loading, since it is determined only by the current values of *n* and *m* in two adjacent cells. It can be obtained by simply coupling two cells with the given occupancies and then averaging over all events that cause a cell to change occupancy from n to $n - 1$ while the other changes from m to $m + 1$. The trend of the probability $W_{n,m}$ with varying n and m (according to $1 \le n \le K$, and $0 \le m \le K - 1$) arises directly from the mathematical structure of both randomization and propagation probabilities defined in eqs 7 and 8, and from the values of the energy parameters (see section 2.1). In Figure 5, curves for the probability of $W_{n,m}$ relative to different values of the occupancy n of the departure cell are plotted vs the occupancy m of the target cell. After small variations at low occupancies, the migration probability decreases rapidly due to a decrease in the availability of the target exit site (a full discussion about this topic can be found in our previous works)[32−34] and due to the fact that high occupancies are unfavorable due to an increased interaction potential (see inset of Figure 3b).

The local parametric structure of our BCA makes it a widely flexible environment where it is easy to modify some properties while leaving untouched the other ones, in order to refine the modeling of a given reference system. For example it is possible to work on the free energy parameters to vary the dependence of diffusivity upon the loading without producing any change in the adsorption isotherm. Such a procedure constitutes a first modeling of the BCAs kinetic behavior, and can be easily realized through (i) modification of the difference $\Delta f^o = f^o_{ex} - f^o_{in}$ (see section 2.1) and (ii) determination of the new function $\phi(n)$ allowing the partition functions $Q(0)$, $Q(1)$, . . ., $Q(K)$ to keep the same values they covered before the modification. As for the above-discussed determination of fitting parameters for Xe in NaA, once a new value of Δf^o is assumed, only one choice of the new interaction parameter $\phi(n)$ will result to be consistent with the fixed values of $Q(n)$. This procedure will produce different diffusion profiles as Δf^o changes (this can be seen in Figure 6), without affecting the global thermodynamic properties of the system. The physical meaning of Δf^o is based upon the knowledge of the probability of a particle to accede to a window; when such an input information is not available, Δf^o can be deduced by adapting the BCA to the kinetic behavior of a particular system. After such a procedure, agreement with reference data can be further improved by adjusting the kinetic barrier ϵ (see eq 8).

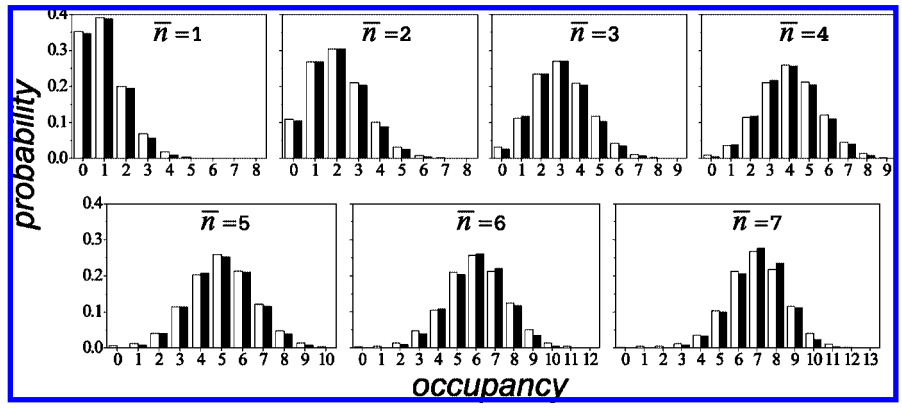

Figure 7. Occupancy probability distributions of our BCA for methane in ZK4 zeolite shown in direct comparison with molecular dynamics simulation data of Fritzsche et al.[38] (white bars).

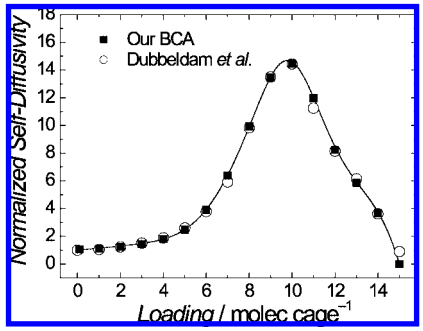

Figure 8. Fit of the MD simulation data of self-diffusion coefficient of methane in ZK4 at 300 K from Dubbeldam et al.[24] with our BCA using the parameters of Table 1. Data are normalized wrt the zero-loading diffusivity.

3.2. Application: Methane in Zeolite ZK4. We take as reference data the occupancy distributions of Fritzsche et al.[38] and the self-diffusion coefficient values reported by Dubbeldam et al.[24]

As can be seen in Figure 7, in order to obtain occupancy distribution trends in agreement with MD data,[38] it is enough to set $K = 15$, $\Delta f^o = 10$ kJ mol^{-1}, and $\phi = 0$ independent of n. In this application we show how the kinetic barrier ϵ can be modeled as a function of the cell occupancy in order to obtain results in good agreement with reference data of diffusivity. In Table 1, we reported the values of k giving the best agreement with MD data[24] shown in Figure 8.

In Figure 9a, we plotted the mean lifetime (MLT) of a cell, that is, how long on average a cell with a given occupancy keeps it unchanged. This quantity is sensitive to the loading (see Demontis et al.[34,54] for a full discussion about this topic), and as one can see by direct comparison between panels a and b of Figure 9, our model captures the qualitative trend found in MD simulations of methane in ZK4 at 360 K.[54] This indicates that our BCA is able to effectively reproduce the essential features of the physical problem under study, from both the thermodynamic and kinetic point of view.

3.3. Application: Ethylene in Zeolite NaA. In this application we take as reference data the adsorption isotherm at 358 K and the self-diffusivity trend at 350 K of Ethylene in zeolite NaA from the experimental data of Ruthven and Derrah[39] and from a Monte Carlo lattice dynamics (MCLD) model developed by Gladden et al.[40] The best set of values for the parameters $\phi(n)$ and $k(n)$ we found to perform the fits reported in Figure 10 is given in Table 1, while the fixed site free energies are set as $f^o_{ex} = -73.126$ kJ mol^{-1} and $f^o_{in} = -79.126$ kJ mol^{-1} and the BCA temperature is 358 K. Besides the fact that our model

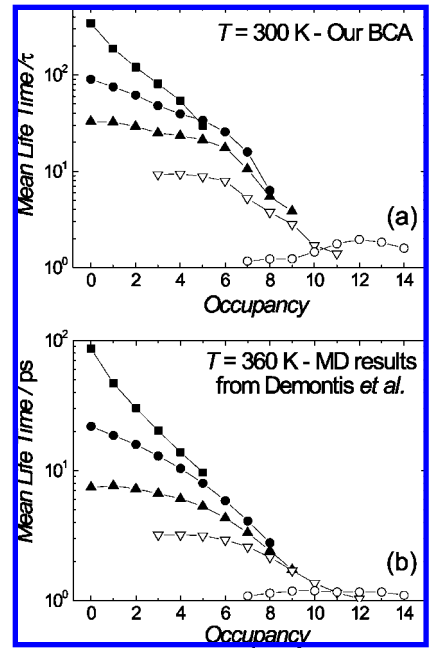

Figure 9. Comparison between (a) BCA and (b) MD results from Demontis et al.[54] for the mean life times of the cells having the most frequent occupancies at various loadings: (■) $\bar{n} = 1$, (●) $\bar{n} = 3$, (▲) $\bar{n} = 5$, (▽)$^-$ $\bar{n} = 7$, (○) $\bar{n} = 11$.

simulates equilibrium and transport properties all at once in the canonical ensemble (see eq 6), we remark an important difference between our approach and the aforementioned MCLD concerning the structure of the single cell: while in a MCLD cell the saturation limit (6 molecules per cell) coincides with the number of exit sites,[40] in a CA cell a nominal maximum occupancy has been set as $K = 8$ in order to make accessible also the inner part of the cell (since $K_{ex} = 6$ due to the LTA topology, we are considering an inner space of $K_{in} = 2$ inner sites). Then, an effective maximum occupancy $K^{eff} = 6$ is imposed via the introduction of a strongly repulsive n-particle potential for occupancies $n > 6$ (i.e., setting $\phi(n > K^{eff}) = \infty$ in eq 3).

This procedure together with $f^o_{in} < f^o_{ex}$ enables the CA cell to mimic the reduced accessibility of exit sites due to the presence of blocking cations on the windows. With this example we emphasize that in our CA, due to the cellular, occupancy-dependent structure of the energetics and to the block synchronous propagation scheme,[27,35] the implementation of a requirement like the constraint on maximum occupancy is straightforward.

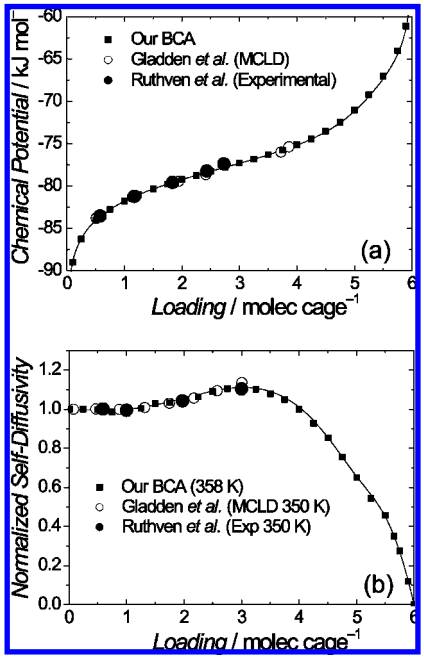

Figure 10. (a) Adsorption isotherm and (b) self-diffusivity profile of ethylene in NaA zeolite obtained by introducing the effective parameters shown in Table 1 into our BCA to fit experimental data of Ruthven and Derrah[39] and Monte Carlo data from Gladden et al.[40]

4. Conclusions

The construction of an efficient BCA able to reproduce the main experimental facts required to identify the basic physics from a detailed analysis of the sorption properties of molecules confined in a zeolite crystal. Two main questions have been taken into account namely (i) how to describe in a meaningful way the microstructure and the pore network connectivity of the zeolite crystal and (ii) how to model the external fields due to the confining geometries. We answered to the first question by mapping the zeolitic framework on a regular geometry of connected and structured pores (cells). The answer to the second question required the BCA to include the proper local interactions in order to reproduce adsorption isotherms and diffusivity. In these systems accurate determination of intermolecular forces to be used in simulations remains a largely unsolved problem and we used the adsorption isotherm to extract the data needed to obtain a mean molecular interaction potential within the cells. In our BCA, the molecules can hop from one cell to another, according to well defined rules satisfying detailed balance, the diffusion coefficient being deduced from their mean square displacement vs time. We have demonstrated that our coarse-grained description representing the microscopic system at the mesoscopic length scale (10−1000 nm) can capture the proper density distribution while retaining microscopic information on particle fluctuations and dynamics. In the pore network modeled in this paper, essentially an LTA type, a molecule can jump from the parent cell to one of the six neighboring cell, and the diffusion behavior will be Einsteinian over time scales that are sufficiently large to allow molecules to move between several coarse-grained cells. On shorter time-scales in a real zeolite, the motion may be more complex, since molecules feel the interactions with the confining walls and possibly with other sorbed molecules within the same cage. The molecules wait in the cage until they gain sufficient energy to move to a neighboring cage. In our BCA, this experimental fact has been reproduced through the action of the inner sites where molecules could be trapped until they are stochastically allowed to gain an exit site. In this way, the necessary computer time can be reduced by orders of magnitude for zeolitic systems where rare event dynamics driven by strong guest−guest and guest−host interactions make full-scale molecular dynamics simulations still prohibitively expensive. We conclude that our BCA can be classified as a mesoscopic dynamical model able to give the correct behavior of various experimental systems that have been investigated in recent years, bringing out very clearly the essential elements involved in the adsorption and diffusion processes. Of course our model cannot replace in any way MD simulations or any other atomistic method in the detailed description of the properties of a complex system like a zeolite since microscopic information about, e.g., the framework composition and the structure of the sorbed molecules is lost. On the contrary, our BCA model can be interpreted as a complementary tool able to retain the essential physical and chemical properties of molecules sorbed in zeolites by averaging over less important detailed information at the atomistic level, which can be acquired through more sophisticated microscopic theoretical approaches and/or experimental measurements. The implementation of a systematic procedure to derive the BCA interaction parameters and kinetic barriers directly from atomistic calculations over a small zeolite's portion would add self-consistency to the model. In this paper we have shown that when constructed from a fitting procedure of experimental data our model is flexible enough to allow a coherent representation of the essential (thermodynamic and dynamic) properties of a host−guest system. Therefore, our BCA can be proposed as a proper environment for a coarse-grained representation of such systems. Moreover, it results that a well-designed coarse-grained description of a microporous material is not simply a way to save computer time, but a route to focus on the main characteristics of sorption and diffusion processes, where details may be unimportant and nonessential.

Acknowledgment. This work has been carried out with financial support provided by Italian Ministero dell'Istruzione, dell'Università e della Ricerca, by Università degli Studi di Sassari, and by Istituto Nazionale per la Scienza e Tecnologia dei Materiali (INSTM), which are acknowledged. This work makes use also of results produced by the Cybersar Project managed by the Consorzio COSMOLAB, a project cofounded by the Italian Ministry of University and Research (MIUR) within the Programma Operativo Nazionale 2000−2006 "Ricerca Scientifica, Sviluppo Tecnologico, Alta Formazione" per le Regioni Italiane dell'Obiettivo 1 (Campania, Calabria, Pugla, Basilicata, Sicilia, Sardegna)−Asse II, Misura II.2 "Società; dell'Informazione", Azione a "Sistemi di calcolo e simulazione ad alte prestazioni". More information is available at http://www.cybersar.it.

References and Notes

(1) van Steen, E.; Callanan, L. H.; Claeys, M., Eds.; *Proceedings of the 14 th International Zeolite Conference*; 2004; ISBN 0−958−46636-X.
(2) Jeong, N. C.; Kim, H. S.; Yoon, K. B. *J. Phys. Chem. C* **2007**, *111*, 10298–10312.
(3) Baerlocher, Ch.; McCusker, L. B.; Olson, D. H. *Atlas of Zeolite Framework Types*; Elsevier: Amsterdam, The Netherlands, 2007.
(4) Treacy, M. M. J.; Higgins, J. B. *Collection of Simulated XRD Powder Patterns for Zeolites*; Elsevier: Amsterdam, The Netherlands, 2007.
(5) Trudu, F.; Tabacchi, G.; Gamba, A.; Fois, E. *J. Phys. Chem. A* **2007**, *111*, 11626–11637.
(6) Smit, B.; Krishna, R. *Curr. Opin. Solid State Mater. Sci.* **2001**, *5*, 455–461.
(7) Demontis, P.; Suffritti, G. B. *Chem. Rev.* **1997**, *97*, 2485–2878.
(8) Smit, B.; Siepmann, J. I. *Science* **1994**, *264*, 1118–1120.
(9) Demontis, P.; Gulin Gonzalez, J.; Tilocca, A.; Suffritti, G. B. *J. Am. Chem. Soc.* **2001**, *123*, 5069–5074.

(10) Ghorai, P. K.; Yashonath, S.; Demontis, P.; Suffritti, G. B. *J. Am. Chem. Soc.* **2003**, *125*, 7116–7123.
(11) Auerbach, S. M.; Jousse, F.; Vercauteren, D. P. In *Computer Modelling of Microporous and Mesoporous Materials*; Catlow, C. R. A.; van Santen, R. A.; Smit, B., Eds.; Elsevier: Amsterdam, 2004; pp 49−108.
(12) Deem, M. W. *AIChE J.* **1998**, *44*, 2569–2596.
(13) Auerbach, S. M. *Int. Rev. Phys. Chem.* **2000**, *19*, 155–198.
(14) Cheung, T. T. P. *J. Phys. Chem.* **1993**, *97*, 8993–9001.
(15) Ayappa, K. G.; Kamala, C. R.; Abinandanan, T. A. *J. Chem. Phys.* **1999**, *110*, 8714–8721.
(16) Ayappa, K. G. *J. Chem. Phys.* **1999**, *111*, 4736–4742.
(17) Güémez, J.; Velasco, S.; Calvo Hernández, A. *Physica A* **1988**, *152*, 243–253.
(18) Güémez, J.; Velasco, S.; Calvo Hernández, A. *Physica A* **1988**, *152*, 226–242.
(19) Saravanan, C.; Jousse, F.; Auerbach, S. M. *Phys. Rev. Lett.* **1998**, *80*, 5754–5757.
(20) Coppens, M.-O.; Bell, A. T.; Chakraborty, A. K. *Chem. Eng. Sci.* **1999**, *54*, 3455–3463.
(21) Krishna, R.; Paschek, D.; Baur, R. *Microporous Mesoporous Mater.* **2004**, *76*, 233–246.
(22) Bhide, S. Y.; Yashonath, S. *J. Chem. Phys.* **1999**, *111*, 1658–1667.
(23) Bhide, S. Y.; Yashonath, S. *J. Phys. Chem. B* **2000**, *104*, 2607–2612.
(24) Dubbeldam, D.; Beerdsen, E.; Vlugt, T. J. H.; Smit, B. *J. Chem. Phys.* **2005**, *122*, 224712.
(25) Tunca, C.; Ford, D. *Chem. Eng. Sci.* **2003**, *58*, 3373–3383.
(26) Boon, J. P.; Dab, D.; Kapral, R.; Lawniczak, A. T. *Phys. Rep.* **1996**, *273*, 55–147.
(27) Toffoli, T.; Margolus, N. *Cellular Automata Machines: A New Environment for Modeling*; MIT Press: Cambridge, MA, 1997.
(28) Chopard, B.; Droz, M. *Cellular Automata Modeling of Physical Systems*; Cambridge University Press: Cambridge, U.K., 1998.
(29) Marechal, M.; Holian, B. L., Eds.; in *Proceedings of the NATO ASI Summer School on: Microscopic simulations of complex hydrodynamic phenomena, held July 15−27, 1991 in Alghero, Sardinia; Chapter III: Lattice Gases*; Plenum Press: New York, 1993; pp 125−238.
(30) Rivet, J.-P.; Boon, J. P. *Lattice Gas Hydrodynamics*; Cambridge University Press: Cambridge, U.K., 2001.
(31) Marro, J.; Dickman, R. *Nonequilibrium Phase Transitions in Lattice Models*; Cambridge University Press: Cambridge, U.K., 1999.
(32) Demontis, P.; Pazzona, F. G.; Suffritti, G. B. *J. Phys. Chem. B* **2006**, *110*, 13554–13559.
(33) Demontis, P.; Pazzona, F. G.; Suffritti, G. B. *J. Chem. Phys.* **2007**, *126*, 194709.
(34) Demontis, P.; Pazzona, F. G.; Suffritti, G. B. *J. Chem. Phys.* **2007**, *126*, 194710.
(35) Toffoli, T.; Margolus, N. *Physica D* **1990**, *45*, 229–253.
(36) Jameson, C. J.; Jameson, A. K.; Baello, B. I.; Lim, H.-M. *J. Chem. Phys.* **1994**, *100*, 5965–5976.
(37) Jameson, A. K.; Jameson, C. J.; Gerald, R. E., II. *J. Chem. Phys.* **1994**, *101*, 1775–1786.
(38) Fritzsche, S.; Haberlandt, R.; Kärger, J.; Pfeifer, H.; Heinzinger, K. *Chem. Phys. Lett.* **1992**, *198*, 283–287.
(39) Ruthven, D. M.; Derrah, R. I. *J. Colloid Interface Sci.* **1975**, *52*, 397–403.
(40) Gladden, L. F.; Sousa-Goncalves, J. A.; Alexander, P. *J. Phys. Chem. B* **1997**, *101*, 10121–10127.
(41) MacQuarrie, D. A. *Statistical Mechanics*; Harper and Row: New York, 1976.
(42) Beenakker, J. J. M.; Kuer, I. *Zeolites* **1996**, *17*, 346–353.
(43) Kuer, I.; Beenakker, J. J. M. *J. Stat. Phys.* **1997**, *87*, 1083–1095.
(44) Kang, H. C.; Weinberg, W. H. *J. Chem. Phys.* **1988**, *90*, 2824–2830.
(45) Hood, E. S.; Toby, B. H.; Weinberg, W. H. *Phys. Rev. Lett.* **1985**, *55*, 2437–2440.
(46) Auerbach, S. M.; Bull, L. M.; Henson, N. J.; Metiu, H. I.; Cheetam, A. K. *J. Phys. Chem.* **1996**, *100*, 5923–5930.
(47) Demontis, P.; Suffritti, G. B. *J. Phys. Chem. B* **1997**, *101*, 5789–5793.
(48) Lim, W. T.; Park, M.; Heo, N. H. *Bull. Korean Chem. Soc.* **2000**, *21*, 75–80.
(49) Jameson, C. J.; Jameson, A. K.; Gerald, R. E., II.; de Dios, A. C. *J. Chem. Phys.* **1992**, *96*, 1676–1689.
(50) Jameson, C. J.; Jameson, A. K.; Baello, B. I.; Lim, H.-M. *J. Chem. Phys.* **1994**, *100*, 5977–5987.
(51) Keffer, D.; McCormick, A. V.; Davis, H. T. *J. Phys. Chem.* **1995**, *100*, 967–973.
(52) Li, F.-Y.; Berry, S. *J. Phys. Chem.* **1995**, *99*, 2459–2468.
(53) Kärger, J.; Ruthven, D. M. *Diffusion in Zeolites and Other Microporous Materials*; John Wiley and Sons: New York, 1992.
(54) Demontis, P.; Fenu, L.; Suffritti, G. B. *J. Phys. Chem. B* **2005**, *109*, 18081–18087.

JP805300Z